DOI: 10.1002/ejic.200700776

Adsorption of Metal Ions on an Activated Carbon/L-Lysine Derivative Hybrid Compound

Javier García-Martín,[a] M. Luz Godino-Salido,[a] Rafael López-Garzón,*[a] M. Dolores Gutiérrez-Valero,[a] Paloma Arranz-Mascarós,[a] and Helen Stoeckli-Evans[b]

Keywords: Adsorption / Ligand design / Transition metals / UV-Vis spectroscopy / Zinc

The new compound N^{ε}-(4-amino-1,6-dihydro-1-methyl-5-nitroso-6-oxopyrimidin-2-yl)-L-lysine (H_2L) has been synthesised and its molecular structure determined by single-crystal X-ray diffraction methods. The Brönsted acid/base character of H_2L has been determined in water in the pH range 2.5–10.0, and the nature of the observed protonation steps determined by potentiometric and spectrophotometric methods. The adsorption of H_2L on a commercial activated carbon (AC) in aqueous solution is irreversible, mainly due to the electronic behaviour of the π system of the pyrimidine moiety. The adsorption of H_2L on the AC provides a route to develop NH_3^+-CHR-COO^--type functions on the AC surface, thereby yielding a new hybrid material with an enhanced adsorption capacity for metal ions in aqueous solution. The adsorption of Ni^{II}, Cu^{II}, Zn^{II} and Cd^{II} ions on the functionalised AC has been studied and the results analysed on the basis of the reactivity data for several pyrimidine ligand/metal ion systems. The results, which show an enhancement of the adsorption capacity of the new material with respect to the unfunctionalised AC, are compared with analogous materials studied previously.

Introduction

The toxicity of metal ions in polluted waters is a serious problem for the safety of living species, especially when tolerance levels are exceeded.[1] For this reason, the search for new technologies for the recovery of metals from wastewaters originating from municipal and industrial activity has become a major topic of research interest.

Adsorption on activated carbon has been shown to be a low-cost and effective method[2–4] to remove low concentrations of metal ions from contaminated water, and a great deal of research has been carried out on this topic in the last few decades to improve the adsorption capacity of activated carbons for the metal ions present in industrial and waste waters.[5–8] It is well known that surface functionalisation of activated carbons improves their adsorption capacity towards metal ions. Thus, considering the specificity of metal ions for certain base donors and coordination environments, the specific functionalisation of carbon surfaces has become a main objective for improving the ability of activated carbons in the metal capture process. This specific functionalisation is difficult to achieve by the usual techniques for activating carbon surfaces as they are rather inefficient when it comes to developing the specific basic functionalities needed for an efficient adsorption of metal ions. We have therefore proposed the anchoring of appropriate molecular receptors on the graphitic surface of the carbon as a good alternative for the development of specific basic functionalities.[9–11] These molecular receptors contain a planar pyrimidine moiety (Ar), which acts as an anchor to attach the receptors onto the arene centres of the activated carbon. This pyrimidine fragment is connected through a polymethylene aliphatic arm (S) to a Lewis base function (F), which acts as an active site for complexation of the metal centres (Scheme 1).

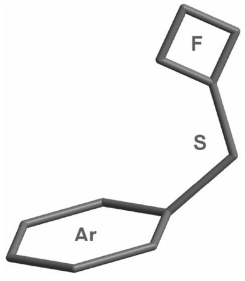

Scheme 1.

Structural studies on these type of derivatives have shown the existence of a strong dipole at the aromatic moieties due to the electron-withdrawing character of their C(5)NO and C(6)O substituents.[12–14] The existence of such a dipole is common to all compounds of this class as the polymethylene separators (S) are not conjugated with the pyrimidine residues. This bipolar character means that the

[a] Dpto. Química Inorgánica y Orgánica, Universidad de Jaén, 23071 Jaén, Spain
[b] Institute of Chemistry, University of Neuchâtel, 2007 Neuchâtel, Switzerland

energy differences between their HOMO and LUMOs are small and that the energy of these orbitals is close to the energy values calculated for the frontier orbitals of modelled arene active sites present on the surface of an activated carbon (AC).[9] This suggests that the observed irreversible adsorption of the above molecular receptors on the AC is probably due to some electron donation, through a π-π interaction, from the arene centres of the carbon to a vacant π orbital of the pyrimidine moiety.

Thus far we have reported the adsorption of seven molecular receptors derived from 4-amino-1-methyl-5-nitroso-6-oxopyrimidin-2-yl, which differ in their C(2) substituents, onto a granular basic H-type AC.[9–11] In the cases of molecular receptors derived from the single amino acids L-alanine, L-valine, L-methionine, L-serine and glycylglycine, the results suggested that the adsorption capacity of the hybrid AC-molecular receptors (AC-MR) to Cu^{II} is better than that of the AC due to the metal-binding capacity of the carboxyl function oft the amino acid moieties.[11] In general, an enhancement of the adsorptive capacity of the AC-MR in relation to the AC is expected if the anchored receptors bear functions (F) with a suitable affinity for the metal ion. The aim of this work is to anchor the new molecular receptor N^{ε}-(4-amino-1-methyl-5-nitroso-1,6-dihydro-6-oxopyrimidin-2-yl)-L-lysine (H_2L), which contains a CO-O^-CHR-NH_3^+-active function and is able to act as stronger bidentate chelating ligand towards metal ions. In order to get further insight into the adsorption behaviour of the chemically modified carbon material we have studied the adsorption capacities of an AC-H_2L hybrid adsorbent towards a series of single bivalent metal ions (Ni^{II}, Cu^{II}, Zn^{II} and Cd^{II}) in aqueous media. The results are analysed on the basis of the reactivity data of the various H_2L/metal ion systems and those of the adsorption of the metal ions on the AC adsorbent.

Results and Discussion

Synthesis and Characterisation of the Molecular Receptor

H_2L was prepared by a synthetic procedure[15] consisting of the condensation of L-lysine and 4-amino-1-methyl-5-nitroso-1,6-dihydro-6-oxopyrimidine[16,17] (see Exp. Sect.). This condensation takes place upon nucleophilic attack of the ε-NH_2 amino group of L-lysine at the C(2) atom of the pyrimidine. For this reason the pH was kept at a constant value to allow the selective protonation of the α-NH_2 group.[18,19]

The structure of H_2L was determined from its 2D ^{1}H-^{1}H, ^{1}H-^{13}C and ^{1}H-^{15}N NMR spectra. The correlation of $C(2)_{pyr}$–N with the ε-CH_2 signals in the latter spectrum (Scheme 2) proved that the lysine residue is connected to the pyrimidine moiety through its ε-NH_2 group.

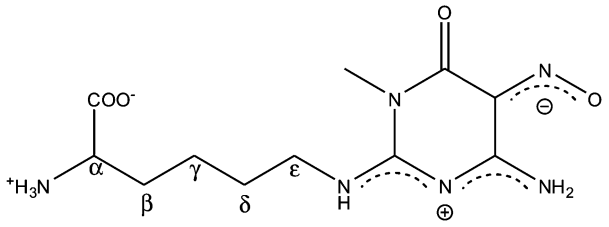

H_2L

Scheme 2.

The structure of $H_2L{\cdot}4H_2O$ was also solved by single-crystal X-ray diffraction methods.[20] A drawing and selected bond lengths of the H_2L unit are shown in Figure 1 and Table 1, respectively. The pyrimidine moiety shows similar structural and electronic features to analogous compounds mentioned above.[12–14]

The C(5)NO group is oriented *trans* to C(6) in such a way that its oxygen atom O(5) is able to form an intramolecular N–H···O hydrogen bond in an S(6) motif, which is coplanar with the pyrimidine ring. However, the N-amino acid side-chain deviates from this plane. The bond lengths in the pyrimidine group are similar to those of analogous derivatives,[12–14] which points to an extensive electronic delocalisation in this moiety. This results in a bipolar character for the pyrimidine with a positive charge located on the NHC(2)N(3)C(4)NH_2 group and a negative one on C(5)NO (Scheme 2). This fact is consistent with the existence of a low-energy LUMO π orbital located at the pyrimidine moiety,[9] which favours a π-π interaction between this moiety and the basic arene centres of the AC that results in irreversible adsorption of the ligand.

In the crystal packing (Figure 1), molecules of H_2L stack with their pyrimidine planes parallel to one another. This arrangement is stabilized by a complex network of inter- and intramolecular hydrogen bonds involving several N and O atoms belonging to H_2L and water molecules. It is also noteworthy that the N_{cyclic} pyrimidine atoms are not involved in the hydrogen-bond network.

Table 1. Selected bond lengths [Å] for $H_2L{\cdot}4H_2O$.

O(1)–N(1)	1.289(3)
O(2)–C(4)	1.230(3)
N(1)–C(1)	1.336(3)
N(2)–C(2)	1.315(3)
N(3)–C(3)	1.325(3)
N(3)–C(2)	1.338(3)
N(4)–C(4)	1.382(3)
N(4)–C(3)	1.386(3)
N(4)–C(5)	1.466(3)
N(5)–C(3)	1.321(3)
C(1)–C(2)	1.445(3)
C(1)–C(4)	1.450(3)

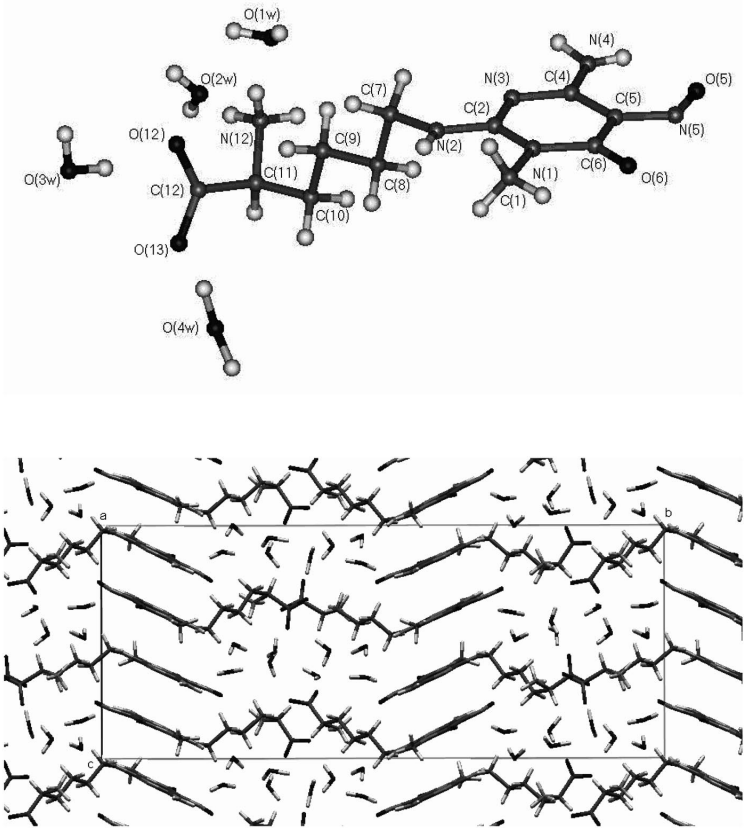

Figure 1. Drawing and packing of $H_2L{\cdot}4H_2O$.

Ligand Protonation

It is important to get an insight into the nature of the various protonated species in solution in order to establish the nature of the complex species in metal ion/H_2L systems. The acid/base behaviour of H_2L (0.1 M KCl, 298.1 K) has already been discussed in a previous work[9] dealing with the adsorption of H_2L aqueous solutions on an AC. H_2L protonation equilibrium constants are collected in Table 2, where it can be seen that the dianion L^{2-} binds up to four protons in the pH range 2.5–11.5. The three latter equilibria were determined by potentiometric techniques (see Exp. Sect.), whereas the first one, which was undetectable by this method, was established by UV and visible spectral measurements.

Table 2. Protonation constants (log K) of the anion L^{2-} (0.1 M KCl, 298.1 K).

Reaction	log K
$H^+ + L^{2-} \rightleftarrows [HL]^-$	>12[a]
$H^+ + [HL]^- \rightleftarrows [H_2L]$	9.24
$H^+ + [H_2L] \rightleftarrows [H_3L]^+$	2.60
$H^+ + [H_3L]^+ \rightleftarrows [H_4L]^{2+}$	2.28

[a] Value obtained by UV/Vis measurements.

The distribution plots of the protonated species of the receptor obtained from the data in Table 2 are shown in Figure 2. The protonation steps of HL^- were studied by ^1H NMR and UV/Vis spectrometric titrations of H_2L in aqueous solution. The protonation of HL^-, which occurs in the pH range 7–11 (Figure 2), is accompanied by an increasing deshielding of the hydrogen atoms of the methylene groups (Figure 3). This deshielding, which is larger as the methylene groups are closer to the NH_2 group of the amino acid moiety, indicates the protonation of the former. This hypothesis is also supported by the fact that the UV/Vis spectrum of H_2L does not change in this pH range (Figure 4), which means that the basic site protonated in this step is not conjugated with the pyrimidine moiety. The stability

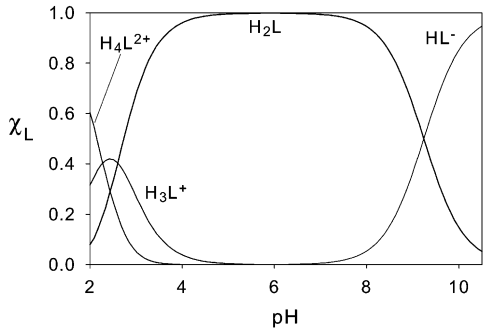

Figure 2. Distribution species diagram (χ_L vs. pH) for the ligand in aqueous 0.1 M KCl solution at 298.1 K.

constant for this process (log K_2 = 9.24) is similar to that of the protonation of the α-amino group of the L-lysine residue.[18,19]

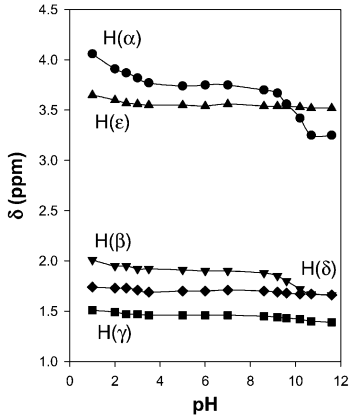

Figure 3. ^{1}H NMR chemical shifts of the H_2L signals as a function of pH.

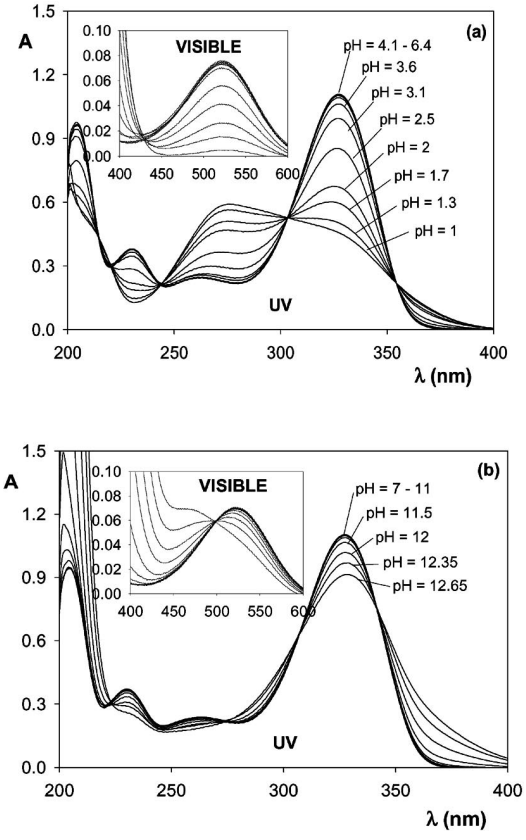

Figure 4. pH-Dependence of the absorption spectra of H_2L in the UV ([H_2L] = 5×10^{-5}M, 0.1 M KCl) and visible (inset; [H_2L] = 10^{-3}M, 0.1 M KCl) regions: a) in an acidic medium; b) in a basic medium.

As shown in Figure 2, neutral H_2L has two overlapping protonation steps in the low pH range (log K_3 = 2.60 and log K_4 = 2.28). The first one, which takes place at pH 5, does not induce any change in the UV/Vis spectrum of H_2L. Moreover, a deshielding of the ^{1}H NMR signals (Figure 3) of the CH_2 groups adjacent to the carboxylate anion of the amino acid residue is produced at this pH. This suggests the protonation of the COO^- anion. Protonation of H_3L^+ starts at a pH of about 4 and is almost complete at pH 1 (90% of H_4L^{2+} is formed at this pH). This process is accompanied by changes in the UV and visible spectra of the compound that indicate protonation of a basic group conjugated with the pyrimidine moiety. Among these changes, the disappearance of the band at 525 nm assigned to a forbidden $n_N \rightarrow \pi^*$ transition of the NO chromophore is worth noting (Figure 4) as it suggests that protonation of H_3L^+ takes place at the nitrogen atom of the mentioned chromophore. A similar behaviour has been reported for the pyrimidine chromophore 2,4-diamino-1-methyl-5-nitroso-1,6-dihydro-6-oxopyrimidine and some of its amino acid derivatives.[21–23]

The deprotonation of HL^- at pH values higher than 11 to form the dianionic species L^{2-} produces changes in the UV and visible spectra, which show isosbestic points at about 500, 345, 305, 275 and 220 nm (Figure 4). This process is not detected by potentiometric measurements because this study was limited to the pH range 2.5–10.0, where the dianion L^{2-} is not formed. Amino acid derivatives analogous to H_2L have also been shown to undergo this process, although in these cases[22] it takes place at pH values of about 9.5, in other words at markedly lower pH, thereby allowing ^{1}H NMR titrations of their aqueous solutions. These results were interpreted as deprotonations involving the C(2)NH_2 attached to the pyrimidine moiety, which suggests that the same also occurs in the case of H_2L.

Complex Formation in Aqueous Solution

As already commented, it has been reported[9] that the adsorption of H_2L on the AC Merck K24504014 takes place by a mechanism consisting of an interaction between the pyrimidine plane of the ligand and the arene centres of the AC. As a result, the chemical reactivity of the AC-MR towards metal ions is likely to be determined by the amino acid residue of the receptor. Thus, the data of the reactivity of H_2L with Ni^{II}, Cu^{II}, Zn^{II} and Cd^{II} ions are important in order to find the experimental conditions under which the amino acid Lewis-base functions of the receptor are operative in adsorption experiments. These studies will also give information about the stability of the amino acid/metal ion complexes that is of great value for interpreting the adsorption capacity of the hybrid AC-MR material for the various metal ions included in this work.

The complex-formation equilibria and the corresponding constants obtained for ligand/metal mixtures in aqueous solutions (0.1 M KCl, 298.1 K) and 1:1 molar ratios were obtained potentiometrically (see Exp. Sect.). The results are listed in Table 3.

As shown in Table 3, the complexes formed in the various metal ion/H_2L systems contain the organic ligand as neutral H_2L, monoanionic HL^-, or dianionic L^{2-} and the metal/organic ligand stoichiometries are very similar in all

Table 3. Stability constants (log K) for Ni^{II}, Cu^{II}, Zn^{II} and Cd^{II} complexes of H_2L (0.1 M KCl, 298.1 K).

Reaction	log K			
	Ni^{II}	Cu^{II}	Zn^{II}	Cd^{II}
$M^{2+} + H_3L \rightleftarrows [M(H_3L)]^{3+}$	–	–	3.20	–
$M^{2+} + H_2L \rightleftarrows [M(H_2L)]^{2+}$	2.98	4.19	2.74	3.63
$M^{2+} + HL^- \rightleftarrows [M(HL)]^{+}$	–	9.07	–	–
$M^{2+} + [M(HL)]^{+} \rightleftarrows [M_2(HL)]^{3+}$	6.33	–	5.06	4.52
$M^{2+} + 2HL^- \rightleftarrows [M(HL)_2]$	–	–	8.82	7.79
$M^{2+} + L^{2-} \rightleftarrows [ML]$	9.75	15.45	–	–
$M^{2+} + L^{2-} + OH^- \rightleftarrows [MLOH]^-$	–	23.64	–	–

the systems. Complexes with the formulae $[M(H_3L)]^{3+}$, $[M(H_2L)]^{2+}$, $[M_2HL]^{3+}$, $[MHL]^{+}$ or $[M(HL)_2]$ and ML are present in the systems.

Mononuclear complexes of the $[M(H_2L)]^{2+}$ type are formed in the low pH range in all metal ion/H_2L systems (Figure 5). Due to the low basicity of the $N(3)_{cyclic}$ atom, the potential binding sites of H_2L are the C(5)NO and C(6)O groups of the pyrimidine (as a monodentate or bidentate-chelating ligand) and the COO^- group of the amino acid residue. Nevertheless, it is expected that the positive charge on the NH_3^+ group of zwitterionic H_2L (which is the counterion of the divalent metal ions M^{2+}) hampers coordination through the COO^- group due to its spatial proximity to the ammonium group. Coordination of neutral H_2L to metal ions through the amino acid function would induce a deshielding of the ^1H NMR signals of the methylene groups adjacent to the amino acid functions.[10] ^1H NMR titrations of H_2L, H_2L/Zn^{II} and H_2L/Cd^{II} solutions in D_2O were carried out to gain an insight into this aspect (see Exp. Sect.). Unfortunately, however, the precipitation of neutral $Zn(HL)_2$ and $Cd(HL)_2$ complexes at pH values up to about 7 did not allow us to extend the measurements to higher pH values. Figure 6 shows the plots of the chemical shifts of the ^1H NMR signals vs. pH for the methylene groups of H_2L, H_2L/Zn^{II} and H_2L/Cd^{II} systems. It can be seen that the methylene protons are unaffected in the presence of metal ions in the pH range 1–7. This means that the ligand is coordinated through the pyrimidine moiety in the main complex species existing in this pH range ($[M(H_2L)]^{2+}$ and $[M(H_3L)]^{3+}$; Figure 5).

The log K values of $[M(H_2L)]^{2+}$ complexes (Table 3) are similar to those of other complexes formed by these metal ions with compounds analogous to H_2L that contain other amino acids as substituents at the $C(2)_{pyr}$ position. Coordination of the ligands in these other complexes takes place in a bidentate-chelating manner, with the nitrogen atom of C(5)NO and the oxygen of C(6)O as binding sites.[22–24]

Monodeprotonation of the ligand NH_3^+ groups of $[M(H_2L)]^{2+}$ complexes and in free (uncoordinated) H_2L molecules start at pH values ranging between 2 (in the case of H_2L/Cu^{II}) and 6 (in the case of H_2L/Cd^{II}; see Figure 5). These values are clearly lower than those for H_2L (approx. 7, Figure 2). In the case of $[M(H_2L)]^{2+}$ species, deprotonation of the ligand occurs concurrently with the attachment of a second metal ion to the amino acid residue of the ligand ($[M(H_2L)]^{2+} + M^{2+} \rightleftarrows [M_2(HL)]^{3+} + H^+$). Deprotonation of free H_2L leads to mononuclear complexes of the type $[M(HL)]^+$ or $[M(HL)_2]$. The presence of a negative charge on the amino acid residue in the HL^- species suggests that the ligands are attached through their amino acid

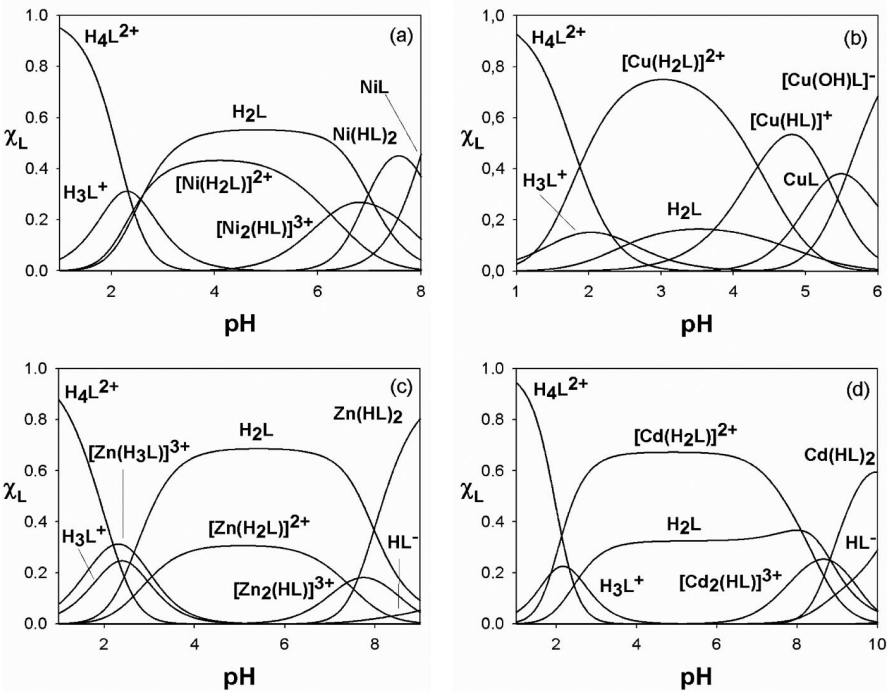

Figure 5. Species distribution diagrams in aqueous solution (H_2L/M^{II} molar ratio 1:1) as a function of pH {$[H_2L] = [M^{II}] = 10^{-3}$ M, 0.1 M KCl, 298.1 K}: a) H_2L/Ni^{II}, b) H_2L/Cu^{II}, c) H_2L/Zn^{II} and d) H_2L/Cd^{II}.

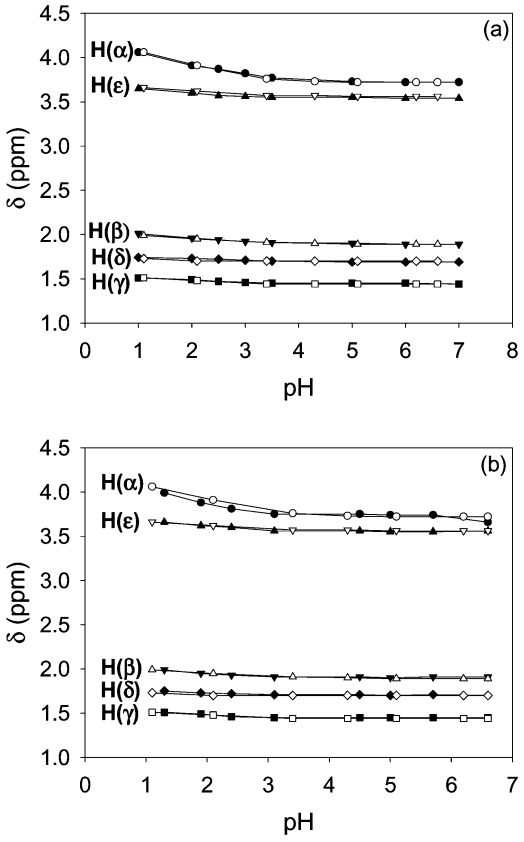

Figure 6. Chemical shifts of the ^{1}H NMR signals corresponding to the methylene protons vs. pH: a) H_2L (black symbols) and 1:1 H_2L/Zn^{II} mixtures (white symbols) and b) H_2L (black symbols) and 1:1 H_2L/Cd^{II} mixtures (white symbols).

residues in the latter complexes. This attachment would explain the highly insoluble nature of $[M(HL)_2]$ complexes, which easily precipitate in all these systems.

The strength of M^{2+}···amino acid interactions can be related to the stability constants of the $M^{2+} + HL^- \rightleftarrows [M(HL)]^+$ equilibrium. However, these equilibria were only detected for the H_2L/Cu^{II} system {$\log K_{[Cu(HL)]^+} = 9.07$; Table 3}. If we assume that the metal ion bonded to the pyrimidine residue in $[M(HL)]^+$ complexes does not affect the binding properties of the amino acid function, the strength of such an interaction can be related to the $\log K_{[M_2(HL)]^{3+}}$ values of the $M^{2+} + [M(HL)]^+ \rightleftarrows [M_2(HL)]^{3+}$ equilibrium. These values can be calculated from the equation $\log K_{[M_2(HL)]^{3+}} = \log \beta_{[M_2(HL)]^{3+}} - \log \beta_{[M(H_2L)]^{2+}} + \log K_{prot}$, where β is the formation constant of the equilibrium ($pM + qL + rH^+ \rightleftarrows M_pH_rL_q$) and $\log K_{prot}$ is relates to the equilibrium $[M(HL)]^+ + H^+ \rightleftarrows [M(H_2L)]^{2+}$, which is assumed to be equal to $HL^- + H^+ \rightleftarrows H_2L$. The $\log K_{[M(H_2L)]^{2+}}$ values obtained are summarised in Table 3. These values are clearly higher than those of the metal complexes formed by analogous amino acid derivatives of glycine, methionine and valine[21–24] in which the amino acid residue has a single carboxylate group as the binding function (F). Nevertheless, the $\log K_{[M(H_2L)]^{2+}}$ values are very similar to, although slightly larger than, those reported for metal complexes of some single amino acids which act as bidentate donors.[19]

The formation of complexes containing the dianion L^{2-} as ligand takes place at pH values that are generally higher than for the formation of complexes of the mono-anionic ligand HL^- in the Ni^{II}/H_2L and Cu^{II}/H_2L systems (Figure 5). The $\log K$ values calculated for L^{2-} complexes (Table 3) are much higher than those for the HL^- ligand (see above). This fact suggests that L^{2-} acts as a tridentate ligand by using the N^- ion attached to C(2) of the pyrimidine together with the NH_2 and COO^- groups of the amino acid moiety. A comparison of the UV spectra of H_2L at pH values different to those of the 1:1 H_2L/Ni^{II} and H_2L/Cu^{II} mixtures shows that binding of NC(2) to metal ions of the latter two produces a strong decrease in the intensity of the band at 327 nm in the H_2L spectrum. This effect is only observed in the pH range at which [ML] and $[CuLOH]^-$ species exist, as can be seen by comparing Figures 5 and 7.

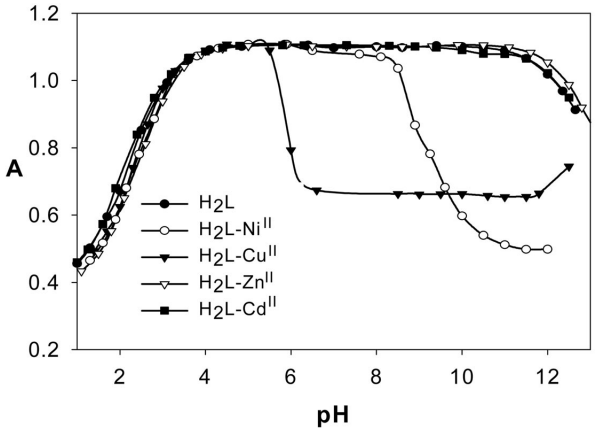

Figure 7. Absorbance values (λ = 327 nm) of H_2L and H_2L/M^{II} mixtures (1:1 molar ratio) in aqueous 0.1 M KCl solution vs. pH.

All these results suggest that H_2L can coordinate to Ni^{II}, Cu^{II}, Zn^{II} and Cd^{II} ions in the whole pH range studied (approx. 2–10). In the low pH range, binding to these metal ions occurs through the C(5)NO–C(6)O function of the pyrimidine moiety. However, the availability of the amino acid function upon deprotonation of NH_3^+ group, at pH values which range between 2 and 6 (for Cu^{II} and Cd^{II}, respectively), determines the formation of the amino acid complexes. The values of $\log K$ for these complexes suggest that this residue acts as a bidentate-chelating ligand to metal ions. The improved adsorptivities of metal ions on the AC upon adsorption of H_2L must therefore be related to the thermodynamic stabilities of such amino acid-metal complexes.

Adsorption of Metal Chlorides

As already commented, the aim of this work is to compare the adsorbent properties of the AC (Merck K24504014) to those of the AC-H_2L hybrid material for a series of divalent metal ions (Ni^{II}, Cu^{II}, Zn^{II} and Cd^{II}). For

this purpose, we obtained the adsorption isotherms of these metal chlorides in aqueous solutions on both adsorbents at various pH values.

Adsorption of Metal Ions on the AC

The AC has already been characterised,[9] and analytical and textural data are summarised in Table 4. This shows the existence of a significant amount of mesopores and macropores.

The analytical data show that oxygen (4.25%) is the only heteroatom species present in a significant amount and that the nitrogen content (0.75%) is negligible. The TPD analysis suggests that most of the oxygen is present as carbonyl, quinone and lactone groups, while a residual amount exists as phenol groups. The XPS diagram of the AC displays two bands in the energy ranges of C_{1s} and O_{1s} electrons. In agreement with the TPD data, the latter band can be decomposed into three signals corresponding to the C=O groups of carbonyl and quinone functions (at 531.7 eV), oxygen atoms of lactone functions (at 533.9 eV) and chemisorbed water (at 537.1 eV; Figure 8 and Table 5).[25–28] Bearing in mind the small proton affinities of carbonyl and lactone functions, the basic character of the AC (pH_{pcz} = 8.3) [9] is mainly due to processes of the type $C_\pi + H_3O^+ \rightleftarrows C_\pi - H_3O^+$.[2]

The adsorption isotherms of Ni^{II}, Cu^{II},[11] Zn^{II} and Cd^{II} aquo ions were obtained at pH values of 2.5, 4.5 and 6.0 (Figure 9).

All these isotherms fit the Langmuir isotherm, with R^2 values ranging between 0.9017 and 0.9988, which allows us to obtain the maximum metal-ion uptakes (X_m). The values obtained are small and range between 0.024(2) and 0.10(2) mmol g^{-1} for Cu^{II} at pH 2.5 and 6, respectively. These small adsorption capacities are consistent with the poor basic functionalisation of the AC surface (Table 4). Metal adsorption results from the interaction of the acidic metal ions with the potential (uncharged at the studied pH values) basic sites on the AC surface. These sites are the oxygen functional groups (which are present in very low amount in this AC)[9] and the basic arene centres of the graphitic surface. However, these metal ions have no affinity in an aqueous medium for most of the oxygen functional groups of the AC, except for carboxylate anions.[19] These anions can appear on the carbon surface due to hydrolysis of the lactone groups,[29] which is expected to be completed in the period of the adsorption experiments (three days). However, the maximum possible amount of such groups (0.011 mmol g^{-1}), as calculated from the CO_2 evolved during TPD of the AC,[9] is very low compared to the maximum ion uptake. Thus, the adsorption of metal ions on the AC is likely to take place through a mechanism consisting of π-d interactions between metals d orbitals and π orbitals of the arene centres (active sites for H^+ in this AC). Similar results have been reported in the case of Cu^{II}-ion adsorption on a low functionalised AC.[2,30] Thus, the small increase in metal-ion uptake as the pH rises (Figure 9 and Table 6) is due not only to a decrease in the positive surface charge, which results in lower electrostatic repulsion be-

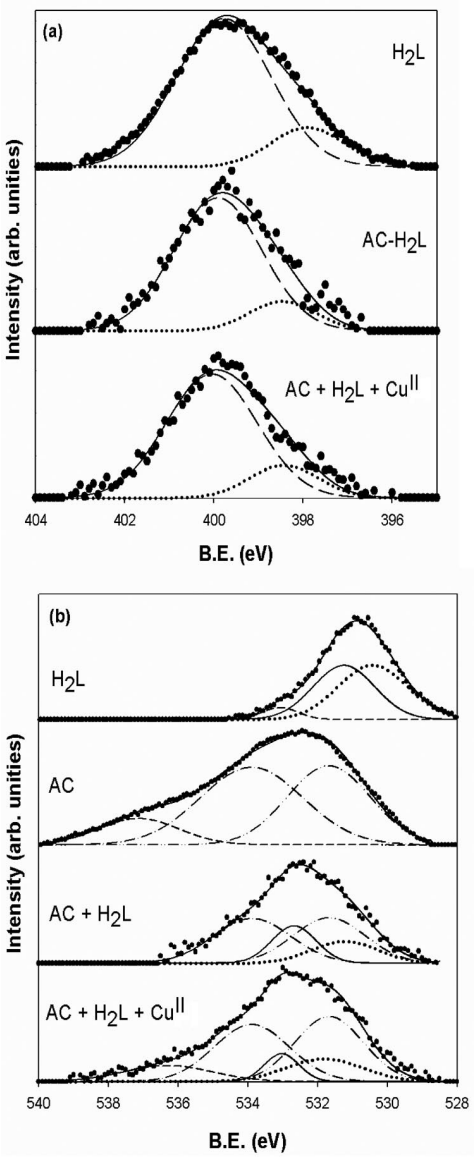

Figure 8. XPS data for H_2L, AC, AC-H_2L and AC-H_2L-Cu^{II} samples: a) N_{1s} signals, the different lines represent: ····· aliphatic, – – – aromatic; b) O_{1s} signals, the different lines represent: ----- H_2O, – – COO^-, ····· C(6)O+C(5)NO, –·–·– COH and –O–, –··–··– C=O (see Table 5).

Table 4. Elemental analysis and textural characteristics of the carbon.

Analysis (%) C	H	N	O[a]	S_{BET} [$m^2 g^{-1}$]	V_{mic} [$cm^3 g^{-1}$]	V_{mes} [$cm^3 g^{-1}$]	V_{mac} [$cm^3 g^{-1}$]	S_{ext} ($m^2 g^{-1}$)	rpm [Å]	Ash (%)
94.70	0.30	0.75	4.25	1000	0.38	0.14	0.24	62	8.3	0.35

[a] Obtained by difference.

Table 5. Binding energies [eV][a] for the O_{1s} and N_{1s} core level spectra.

Sample	O_{1s}					N_{1s}	
	H_2O	Compound		Carbon			
		COO^-	C(6)O+C(5)NO	COH^+ and –O–	C=O	$N_{arom.}$	$N_{aliph.}$
AC	537.1	–	–	533.9	531.7	–	–
H_2L	533.0	531.2	530.4	–	–	399.7	397.9
AC-H_2L	–	532.6	531.3	533.9	531.7	399.9	398.5
AC-H_2L-Cu^{II}	536.3	533.1	531.7	533.9	531.7	400.0	398.4

[a] The variation in the last digit is ±2 units for all values (see Exp. Sect.).

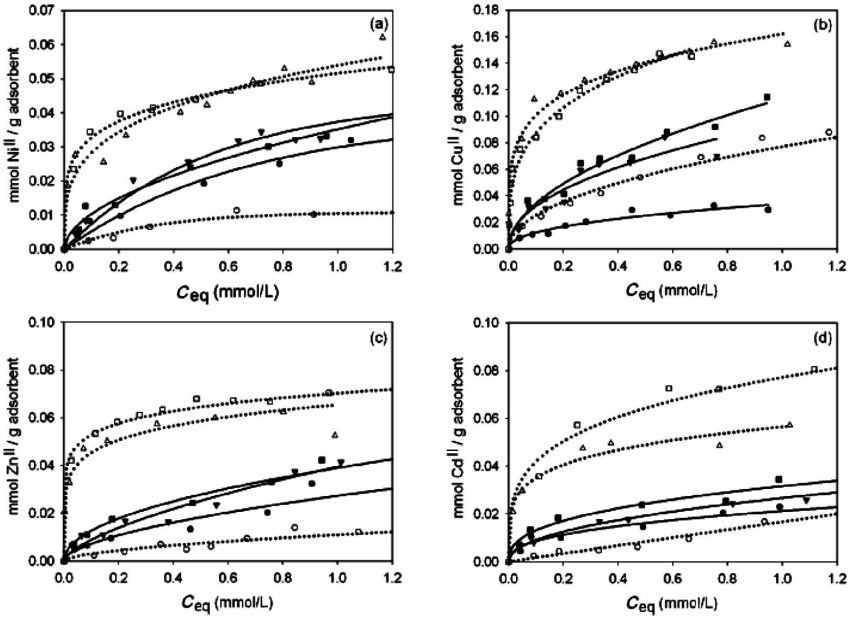

Figure 9. Adsorption isotherms of $M^{II}_{aq.}$ ions (a: Ni^{II}, b: Cu^{II}, c: Zn^{II} and d: Cd^{II}) on AC (black symbols and solid lines) and AC-H_2L (white symbols and dotted lines) at pH 2.5 (●/○), 4.5 (▼/△) and 6.0 (■/□).

Table 6. Maximum metal ion adsorption capacities [mmol g^{-1}] on AC and AC-H_2L and the respective Langmuir constants (K_L, in square brackets).

pH	Adsorbent: AC				Adsorbent: AC-H_2L			
	Ni^{II}	Cu^{II}	Zn^{II}	Cd^{II}	Ni^{II}	Cu^{II}	Zn^{II}	Cd^{II}
2.5	0.038(9)	0.024(6)	0.034(8)	0.025(5)	0.014(2)	0.08(1)	0.020(5)	0.03(1)
	[2.4(7)]	[11(5)]	[2.6(9)]	[5(2)]	[2.4(7)]	[5(1)]	[1.2(4)]	[1.0(5)]
4.5	0.049(2)	0.09(2)	0.05(2)	0.035(3)	0.060(3)	0.153(4)	0.059(2)	0.051(4)
	[2.7(1)]	[6(2)]	[1.9(9)]	[3(24)]	[6(1)]	[26(3)]	[61(8)]	[46(9)]
6.0	0.05(2)	0.10(2)	0.051(6)	0.036(3)	0.060(2)	0.166(6)	0.072(1)	0.096(3)
	[3(2)]	[6(2)]	[3.2(6)]	[6(1)]	[6(1)]	[10(1)]	[24(2)]	[5.4(4)]

tween the charge and the metal ion, but also to a decrease in competition between metal ion species and protons for arene centres (basic sites for the protons in this AC).

Adsorption of Metal Ions on the AC-H_2L

The adsorption isotherms of the metal ions on the AC-H_2L hybrid in aqueous solution were also obtained at pH values of 2.5, 4.5 and 6.0. AC-H_2L was prepared by adsorption of a 3×10^{-3} M aqueous solution of H_2L on the AC at 298.1 K and pH 7. These conditions are those for maximum surface coverage without any desorption of the ligand at the working pH values.

The maximum metal ion concentration used to obtain each pH isotherm was selected taking into account the species distribution plots of the metal ions in aqueous media as a function of pH[31] to be sure that the only metal species present over the whole concentration range was the aquo ion. All the equilibrium solutions were analysed by UV and visible spectroscopy to check that the ligand was not desorbed during the experiments. When these experiments were carried out at pH 2.5, this pH was reached by adding HCl to the metal-ion solutions and it was checked that, even at the maximum chloride ion concentrations used, formation of chloride-metal ion species was negligible.[32]

The adsorption mechanism of H_2L on the AC has been established in a previous work on the basis of the data from adsorption and desorption isotherms and those of MO calculations.[9] Further insight into this mechanism can be obtained by analysing the XPS data in Figure 8. The O_{1s} band of H_2L is composed of two signals corresponding to the aromatic oxygen atoms C(5)NO and C(6)O at 530.4 eV and the aliphatic carboxyl group at 531.2 eV. The N_{1s} band also consists of two overlapping signals at 399.7 eV, which are assigned to the five aromatic nitrogen atoms, and the aliphatic NH_3^+ group at 397.9 eV. The XPS plot of AC-H_2L has three bands in the energy ranges corresponding to C_{1s}, O_{1s} and N_{1s} electrons. The O_{1s} band is composed of four signals (Figure 8), two of which are assigned to the carbonyl groups and lactone functions of the carbon surface and are at the same energy values as in the XPS diagram of the AC (see above and Figure 8); the other two bands (at 531.3 and 532.6 eV) are due to the aromatic and aliphatic oxygens of H_2L, respectively. The former is shifted to higher energy with respect to H_2L, which is consistent with some electron donation from the arene centres to the pyrimidine moiety upon anchoring H_2L on the AC surface. The shift of the COO^- signal reflects the change in the environment of this function upon adsorption of the ligand. It is noteworthy that the oxygen signal of the water anchored at the arene centres, which is present in the XPS plot of the AC, does not appear in that of AC-H_2L. This suggests that water is removed from the arene centres to solution when H_2L is adsorbed onto the AC surface. Moreover, the XPS spectrum of AC-H_2L has a band at 399.4 eV which is assigned to N_{1s} electrons. This band, which is absent in the XPS diagram of the AC, due to its negligible amount of nitrogen, is composed of two signals: one at 399.9 eV, which corresponds to the five aromatic nitrogen atoms, and the other, at 398.5 eV, due to the amino group of the amino acid. These two signals also appear in the H_2L spectrum but shifted to higher energies (Figure 8). This shift has no physical meaning in the case of the amine group due to its participation in hydrogen bonding, which gives rise to the characteristic supramolecular assembly of solid H_2L (Figure 1). Nevertheless, the shift in the case of the aromatic nitrogen atoms suggests some electron donation from the arene centres of the AC to the aromatic residue of H_2L.

The above-mentioned data are consistent with the hypothesis that H_2L is adsorbed on the AC surface by a π-π interaction between the pyrimidine moiety of the adsorbate and the arene centres of the adsorbent.[9] This adsorption mechanism blocks the C(5)NO–C(6)O basic functions, which are not available for metal ion complexation, while providing NH_3^+-CHR-COO^- functions with chelate complexing properties for metal ions at the graphitic surface (see above).

The adsorption isotherms of Ni^{II}, Cu^{II}, Zn^{II} and Cd^{II} ions on AC-H_2L are shown in Figure 9. The isotherms were obtained at pH values of 2.5, 4.5 and 6.0 for each metal ion. The experimental data can be fitted to Langmuir-type functions in all cases, with R^2 factors varying between 0.9117 and 0.9929. This allows the maximum metal adsorption capacities of AC-H_2L, which are summarised in Table 6, to be calculated.

The data in Figure 9 and Table 6 show that adsorption of the ligand on the carbon surface enhances the adsorption capacity of the AC for all the metal ions studied at pH 4.5 and 6.0, whereas it is clearly smaller for all the metal ions, except for Cu^{II}, at pH 2.5.

The XPS diagrams of AC-H_2L-Cu^{II} were obtained to gain an insight into the nature of these adsorption processes (Figure 8). The sample was prepared by adsorption of Cu^{II} from aqueous solution onto AC-H_2L at a pH of around 5. The presence of the N_{1s} signal at similar energy values in the XPS diagrams of AC-H_2L-Cu^{II} and AC-H_2L suggests that the improvement in the adsorption capacity of AC-H_2L with respect to that of AC is due to functionalisation of the AC by H_2L.

The similarity between the energy values of the N_{1s} signals of the non-aromatic amino groups of AC-H_2L-Cu^{II} and AC-H_2L (Figure 8 and Table 5) points to similar electronic environments for the N atoms of both amino groups. This is consistent with the fact that those NH_2 groups are bonded to a proton in the case of AC-H_2L, whereas they are linked to the metal ion in AC-H_2L-Cu^{II}. It is worth mentioning that the COO^- signal of AC-H_2L-Cu^{II} is shifted to higher energy by 0.50 eV, which suggests a Cu^{II}-COO^- interaction similar to that reported for analogous amino acid receptors.[11] The O_{1s} band of AC-H_2L-Cu^{II} also contains a signal due to water molecules, which are probably coordinated to the metal ion. Thus, the XPS data suggest that the improvement of the adsorption capacity of AC-H_2L with respect to that of AC is due to the presence of H_2L on the carbon surface.

The results of these adsorption studies can also be explained on the basis of the adsorption mechanism of H_2L on the AC, as described above. The almost negligible maximum adsorption capacity of AC-H_2L at pH 2.5 is consistent with the fact that the amino group of the NH_3^+-CHR-COO^- function is fully protonated at this pH, except in the case of the Cu^{II} ion (Figure 5). Moreover, a large number of arene centres (another possible basic site for metal ions) are blocked by the anchored receptor molecules, which explains the smaller metal ion adsorption capacity of AC-H_2L at this pH compared to that of the AC. These results also suggest that the other available functions [C(5)NO–C(6)O] for metal ion complexation, which are co-planar with the pyrimidine ring, are blocked due to a plane-to-plane interaction between the ligand and the arene centres of the AC, which does not allow metal coordination to these functions.

The increase in the maximum adsorption capacity for all metal ions as the pH increases from 2.5 to 4.5 is due to an increase of the induced deprotonation of the zwitterionic residue, which allows a higher metal chelating complexation with the NH_2-CHR-COO^- function. The small increase in the formation of metal complex species of this function, as observed in the distribution plots of the ligand/metal systems when the pH increases from 4.5 to 6.0, is also consistent with the small differences observed between the maximum adsorption capacities at pH 4.5 and 6.0. It is also

significant that the trend in the maximum adsorption capacities follows the Irving–Williams sequence[33] $Ni^{II} < Cu^{II} > Zn^{II}$, which is consistent with the complex formation mechanism proposed.

Although the COO^--CHR-NH_2 chelating function in the anchored H_2L ligand forms more stable complexes with Cu^{II} {$\log K_{[Cu(HL)]^+} = 9.07$} than the COO^- moiety in the five amino acid (AA) derivatives already reported ($\log K_{Cu-AA} \approx 3.4$),[11] the maximum adsorption capacities for this ion obtained with the latter receptors (0.18 mmol g^{-1} at the most favourable pH of around 4[11]) are almost equal to those obtained with H_2L at the best pH value (approx. 4.5; see above). This is due to the fact that the COO^--CHR-NH_2 group in H_2L is not available at pH 4.5 (Figure 5), whereas all the COO^- groups in the single amino acids are available at pH 4.

Conclusions

The molecular structure of H_2L shows that the pyrimidine moiety has a bipolar character, which was already stated as the source of its irreversible adsorption on the low-functionalised AC used in this work. This adsorption takes place by a plane-to-plane interaction between the pyrimidine moiety and the arene centres. The XPS data are consistent with this mechanism. The adsorption of H_2L provides a route to develop COO^--CHR-NH_2 functionalities on the graphitic surface of the AC. This function forms five-membered chelate complexes with Ni^{II}, Cu^{II}, Zn^{II} and Cd^{II} metal ions in aqueous solutions whose $\log K_{[M(HL)]^+}$ values suggest higher stabilities than those corresponding to analogous receptors with only COO^- complexing functions.

AC-H_2L has a higher adsorption capacity than the original AC at pH values above those corresponding to the beginning of the deprotonation of the COO^--CHR-NH_3^+ function, whereas at pH 2.5, where the ligand function is protonated (except in the case of Cu^{II}), AC-H_2L shows a smaller adsorption capacity than the AC for all metal ions studied, except Cu^{II}. These latter results confirm the unavailability of the C(5)NO–C(6)O function as a consequence of the adsorption mechanism.

The changes in the adsorption capacities with pH are consistent with the change of the complexing ability of the COO^--CHR-NH_3^+ function with pH, whereas the adsorption capacities for the metal ions studied at a given pH follow the trend expected due to the complexing ability of this function for these metal ions. It is noteworthy that, at the maximum pH values studied, which are limited in order to have only metal aquo ions in solution, the potential maximum efficiency of the receptor is limited because some of the strongly basic amino groups of the receptor remain protonated.

These results continue our work on the design of new receptors of this class in order to gain efficiency in metal-ion adsorption and to carry out further adsorption studies that will allow us to gain a better knowledge of the factors influencing the irreversible character of the carbon–ligand interactions.

Experimental Section

Synthesis of N^{ε}-(4-Amino-1-methyl-5-nitroso-1,6-dihydro-6-oxopyrimidin-2-yl)-L-lysine (H_2L): L-Lysine hydrochloride (29.7 mmol, 5.494 g) and 4-amino-1-methyl-2-methoxy-5-nitroso-1,6-dihydro-6-oxopyrimidine (27.2 mmol, 5.494 g) were suspended in an aqueous 0.2 N KOH solution (160 mL) and the mixture heated at 70 °C for an hour until a pink solid precipitated. This solid was filtered off and washed with ethanol and diethyl ether before being used without further purification. Yield: 7.274 g (75%). $C_{11}H_{18}N_6O_4 \cdot 1.5H_2O$ (325.31): calcd. C 40.61, H 6.51, N 25.83; found C 40.26, H 6.77, N 25.39. ^{15}N-^1H HMBC ([D$_6$]DMSO): δ = 42, 95, 105, 135, 170 ppm. ^1H NMR ([D$_6$]DMSO): δ = 1.43 (2 H), 1.61 (2 H), 1.77 (2 H), 3.22 (2 H), 3.37 (3 H), 3.45 (2 H), 10.87 (2 H) ppm. ^{13}C NMR ([D$_6$]DMSO): δ = 21.9, 27.3, 28.1, 30.0, 40.0, 54.0, 142.7, 150.3, 154.6, 161.8, 171.1 ppm.

X-ray Crystallography: Suitable crystals of $C_{11}H_{18}N_6O_4 \cdot 4H_2O$ ($H_2L \cdot 4H_2O$) were obtained as red blocks by re-crystallisation of H_2L from aqueous solution. Crystal data and details of the structure determination are included in Table 7. Intensity data were collected at 153 K (–120 °C) on a Stoe Mark II-Image Plate Diffraction System[34] equipped with a two-circle goniometer and using graphite-monochromated Mo-K_α radiation. Image plate distance: 100 mm; ω rotation scans: 0–180° at ϕ = 0° and 0–90° at ϕ = 90°; step $\Delta\omega$: 1.0°; 2θ range: 2.29–59.53°; d_{min}/d_{max}: 17.779/0.716 Å.

Table 7. Crystal data and structure refinement for $H_2L \cdot 4H_2O$.

Empirical formula	$C_{11}H_{26}N_6O_8$
Formula mass	370.38
Temperature [K]	153(2)
Wavelength [Å]	0.71073
Space group	$P2_1$
a [Å]	7.5413(3)
b [Å]	31.5845(19)
c [Å]	14.7114(6)
α [°]	90
β [°]	98.103(3)
γ [°]	90
V [Å^3]	3469.1(3)
Z	8
Calcd. density [g cm^{-3}]	1.418
Linear absorption coefficient [mm^{-1}]	0.120
Crystal size [mm]	0.30 × 0.30 × 0.23
Final R indices [$I > 2\sigma(I)$][a]	R_1 = 0.0531, wR_2 = 0.1158
R indices (all data)[a]	R_1 = 0.0815, wR_2 = 0.1269

[a] $R_1 = \Sigma||F_o| - ||F_c||/\Sigma|F_o|$; $wR_2 = [\Sigma w(F_o^2 - F_c^2)^2/\Sigma wF_o^4]^{1/2}$.

The structure was solved by direct methods with the program SHELXS-97.[35] Refinement and all further calculations were carried out with SHELXL-97.[36] All H-atoms were located from Fourier difference maps, however C–H hydrogen atoms were included in calculated positions and treated as riding atoms using the SHELXL default parameters. N–H hydrogen atoms were refined isotropically, except for H8X, for which the N8–H8X distance was restrained to be 0.91(2) Å. The O–H distance was restrained to be 0.90(5) Å and U_{iso}(H) = 1.5 U_{eq} (O atom) for some water molecules; the remainder were refined isotropically. Non-H atoms were refined anisotropically using a weighted full-matrix least-squares procedure on F^2.

CCDC-652608 contains the supplementary crystallographic data for this paper. These data can be obtained free of charge from The Cambridge Crystallographic Data Centre via www.ccdc.cam.ac.uk/data_request/cif.

XPS Data: XPS diagrams for AC, AC-H_2L and AC-H_2L-Cu^{II} were obtained with a VG-Microtech Multilab electron spectrometer using Mg-K_α (1253.6 eV) radiation from a twin anode in the constant analyser energy mode with a pass energy of 50 eV. The analysis chamber pressure was kept at 5×10^{-10} mB. The binding energy and Auger kinetic energy scale were regulated by setting the C_{1s} transition at 284.6 eV. The accuracy of the BE values was ±0.2. The spectra obtained after background signal correction were fitted to Lorentzian and Gaussian curves[37] in order to obtain the number of components, the BE values of each peak and the peak areas.

Spectrophotometric Measurements: UV/Vis spectra of H_2L and H_2L/M^{II} (1:1 molar ratio) in aqueous solution (0.1 M KCl) were recorded with a Perkin–Elmer Lambda 19 spectrophotometer. HCl and KOH were used to adjust the pH values, which were measured with a Crison 2002 micro-pH meter.

NMR Spectroscopy: ^1H (300.13 MHz), ^{13}C (75.48 MHz) and two-dimensional spectra of D_2O solutions at different pH values were recorded at 300 K with a Bruker DPX300 spectrometer. The pD values of H_2L and H_2L/metal ion solutions were adjusted by adding small amounts of NaOD and DCl solutions. The pH was calculated from the measured pD values using the formula pH = pD – 0.40.[38]

Potentiometric Measurements: Potentiometric titrations of metal/ligand mixtures in aqueous solution were carried out at 298.1 ± 0.1 K in 0.1 M aqueous KCl solution with a 713 Metrohm pH-mV meter equipped with a combined glass electrode and connected to a Metrohm 765 Dosimat autoburette (1 ± 0.001 mL). The experimental procedure has been described elsewhere.[39] Typically, $1–1.5 \times 10^{-3}$ M ligand concentrations and 1:1 ligand/metal molar ratios were employed in potentiometric measurements. At least four titration experiments (150 data points each one) were carried out in the pH range between 2.5 and 10.0. The HYPERQUAD software package[40] was used to calculate the equilibrium constants from the EMF data.

Adsorption Studies: A granulated activated carbon (AC, Merck K24504014) was used for adsorption studies. Elemental analyses, surface area, porosity, nature of oxygen-containing groups, and proton isotherms (to obtain the point of zero charge, pHPZC) were obtained as reported.[9,11]

Adsorption isotherms of MCl_2 salts in aqueous solutions on the AC and AC-H_2L adsorbents were obtained at 298.1 ± 0.1 K. Typically, 0.0500 g of the adsorbent was added to a 100-mL plastic flask containing 50 mL of the appropriate aqueous solution of the adsorbate. Experiments were carried out at several pH values, which were initially adjusted with KOH or HCl. To carry out the adsorption of metal ions on the AC-H_2L adsorbent, it was necessary to prepare the latter previously. This preparation was done by an adsorption experiment of a H_2L solution on the AC at the maximum ligand concentration corresponding to 100% of irreversible adsorption (5.0000 g of the AC with 1 L of a 3 mM solution of H_2L at pH 7).[9]

In the adsorption experiments of metal ions with the AC-H_2L adsorbent, it was also checked that none of the ligand H_2L was desorbed in the equilibrium solutions.

Acknowledgments

The authors thank the Spanish Ministerio de Educación y Ciencia (MEC) for financial support (project no.: PPQ 2000/1667).

[1] *World Health Organisation International Standards for Drinking Water*, WHO, Geneva, **1971**.
[2] L. Radovic, C. Moreno-Castilla, J. Rivera-Utrilla, in *Chemistry and Physics of Carbon* (Ed.: L. Radovic), Marcel Dekker, New York, **2000**, vol 27, p. 241–283.
[3] S. D. Faust, O. M. Aly, *Chemistry of Water Treatment,* Ann Arbor Press, Chelsea, **1998**.
[4] S. D. Faust, O. M. Aly, *Adsorption Processes for Water Treatment*, Butterworths, Boston, **1987**.
[5] P. A. Brown, S. A. Gill, S. J. Allen, *Water Res.* **2000**, *34*, 3907–3916.
[6] K. Csobán, M. Párkányi-Berka, P. Joó, Ph. Behra, *Colloids Surf. A* **1998**, *141*, 347–364.
[7] K. Kadirvelu, C. Namasivayam, *Environ. Technol.* **2000**, *21*, 1091–1097.
[8] A. M. Puziy, A. I. Poddubnaya, A. Martínez-Alonso, F. Suárez-García, J. M. D. Tascón, *Carbon* **2002**, *40*, 1493–1505.
[9] J. García-Martín, R. López-Garzón, M. L. Godino-Salido, M. D. Gutiérrez-Valero, P. Arranz-Mascarós, R. Cuesta, F. Carrasco-Marín, *Langmuir* **2005**, *21*, 6908–6914.
[10] J. García-Martín, R. López-Garzón, M. L. Godino-Salido, R. Cuesta-Martos, M. D. Gutiérrez-Valero, P. Arranz-Mascarós, H. Stoeckli-Evans, *Eur. J. Inorg. Chem.* **2005**, 3093–3103.
[11] M. D. Gutiérrez-Valero, M. L. Godino-Salido, P. Arranz-Mascarós, R. López-Garzón, R. Cuesta, J. García-Martín, *Langmuir* **2007**, *23*, 5995–6003.
[12] J. N. Low, M. D. López, P. Arranz-Mascarós, J. Cobo-Domingo, M. L. Godino-Salido, R. López-Garzón, M. D. Gutiérrez-Valero, M. Melguizo, G. Ferguson, C. Glidewell, *Acta Crystallogr., Sect. B* **2000**, *56*, 882–892.
[13] J. N. Low, A. Quesada, C. Glidewell, M. A. Fontecha, P. Arranz, M. L. Godino-Salido, R. López-Garzón, *Acta Crystallogr., Sect. E* **2002**, *58*, 942–945.
[14] M. L. Godino-Salido, P. Arranz-Mascarós, R. López-Garzón, M. D. Gutiérrez-Valero, J. N. Low, J. F. Gallagher, C. Glidewell, *Acta Crystallogr., Sect. B* **2004**, *60*, 46–64.
[15] M. Melguizo, A. Marchal, M. Nogueras, A. Sánchez, J. N. Low, *J. Heterocycl. Chem.* **2002**, *39*, 97–103.
[16] M. Engelman, *Ber. Dtsch. Chem. Ges.* **1909**, *42*, 177.
[17] J. Lifschitz, *Ber. Dtsch. Chem. Ges.* **1922**, *55*, 1619.
[18] O. Yamauchi, A. Odani, *Pure Appl. Chem.* **1996**, *68*, 469–496.
[19] A. E. Martell, R. M. Smith, R. J. Motekaitis, *NIST Critically Stability Constants of Metal Complexes Database*, version 7, Texas A & M University, College Station, TX, **2003**.
[20] PLATON/PLUTON, version Jan. **1999**: A. L. Spek, *Acta Crystallogr., Sect. A* **1999**, *46*, C-34.
[21] R. López-Garzón, P. Arranz-Mascarós, M. L. Godino-Salido, M. D. Gutiérrez-Valero, R. Cuesta, J. M. Moreno, *Inorg. Chim. Acta* **2003**, *355*, 41–48.
[22] R. López-Garzón, M. L. Godino-Salido, P. Arranz-Mascarós, M. A. Fontecha-Cámara, M. D. Gutiérrez-Valero, R. Cuesta, J. M. Moreno, H. Stoeckli-Evans, *Inorg. Chim. Acta* **2004**, *357*, 2007–2014.
[23] J. M. Moreno, P. Arranz-Mascarós, R. López-Garzón, M. D. Gutiérrez-Valero, M. L. Godino-Salido, J. Cobo-Domingo, *Polyhedron* **1999**, *18*, 1635–1640.
[24] R. López-Garzón, P. Arranz-Mascarós, M. L. Godino-Salido, M. D. Gutiérrez-Valero, A. Pérez-Cadenas, J. Cobo-Domingo, J. M. Moreno, *Inorg. Chim. Acta* **2000**, *308*, 59–64.
[25] C. D. Wagner, W. M. Riggs, L. E. Davis, J. F. Moulder, G. E. Muilenberg, in *Handbook of X-ray Photoelectron Spectroscopy*, Perkin–Elmer Corporation, Physical Electronics Division, Eden Prairie, MN, **1979**, p. 38.
[26] K. László, A. Szücs, *Carbon* **2001**, *39*, 1945–1953.
[27] A. R. Silva, C. Freire, B. de Castro, M. M. A. Freitas, J. L. Figueiredo, *Microporous Mesoporous Mater.* **2001**, *46*, 211–221.
[28] D. Lennon, D. T. Lundie, S. D. Jackson, G. J. Kelly, S. F. Parker, *Langmuir* **2002**, *18*, 4667–4673.

[29] J. March, *Advanced Organic Chemistry*, 4th ed., Wiley-Interscience, New York, **1992**.
[30] S. Biniak, M. Pakula, G. S. Szymansky, A. Swiatkowski, *Langmuir* **1999**, *15*, 6117–6122.
[31] C. F. Baes, R. E. Mesmer, *The Hydrolysis of Cations*, J. Wiley & Sons, New York, **1986**.
[32] *Comprehensive Inorganic Chemistry*, vol. 3, 1st ed. (Eds.: J. C. Bailar, H. J. Emeléus, R. Nyholm, A. F. Trotman-Dickenson), Pergamon Press, Oxford, New York, **1973**.
[33] C. E. Housecroft, A. G. Sharpe, *Inorganic Chemistry*, 2nd ed., Pearson Education Limited, Harlow, **2005**, pp. 587–588.
[34] Stoe & Cie, X-Area V1.17 & X-RED32 V1.04 Software, Stoe & Cie GmbH, Darmstadt, Germany, **2002**.
[35] SHELXS-97 Program for Crystal Structure Determination: G. M. Sheldrick, *Acta Crystallogr., Sect. A* **1990**, *46*, 467–473.
[36] G. M. Sheldrick, *SHELXL-97*, University of Göttingen, Germany, **1999**.
[37] R. Kwok, *XPSPEAK, XPS peak fitting program*, University of Hong Kong, **2000**.
[38] A. K. Covington, M. Paabo, R. A. Robinson, R. G. Bates, *Anal. Chem.* **1968**, *40*, 700–706.
[39] M. L. Godino-Salido, M. D. Gutiérrez-Valero, R. López-Garzón, J. M. Moreno-Sánchez, *Inorg. Chim. Acta* **1994**, *221*, 177–181.
[40] P. Gans, A. Sabatini, A. Vacca, *Talanta* **1996**, *43*, 1739–1753.
Received: July 23, 2007
Published Online: January 7, 2008

